

# Large-eddy simulations of turbulent reacting stagnation point flows

**Thomas M. Smith**

*Georgia Inst. of Technology, Atlanta*

**S. Menon**

*Georgia Inst. of Technology, Atlanta*

**AIAA, Aerospace Sciences Meeting & Exhibit, 35th, Reno, NV, Jan. 6-9, 1997**

A methodology for solving unsteady premixed turbulent flame propagation problems in high Reynolds number ( $Re$ ), high Damkohler number spatially evolving flows is developed. The method is based on Large-Eddy Simulation (LES) with a subgrid combustion model based on the Linear-Eddy Model (Kerstein, 1991). An inter-LES cell burning mechanism has been added to the present formulation to account for molecular diffusion (burning) across LES cells which was been neglected in earlier studies. Two-dimensional simulations of passive isotropic flame propagation using the LES-LEM for  $Re$  from 100 to 1000 are conducted to validate the subgrid and supergrid propagation mechanisms. Two models are used to simulate turbulent premixed stagnation point flames. The first model is a conventional approach which uses a thin flame model (Kerstein et al., 1988) with and without significant heat release. The second model uses the LES-LEM approach without heat release. Qualitative comparisons between simulations and experimental data are made. (Author)

# Large-Eddy Simulations of Turbulent Reacting Stagnation Point Flows \*

Thomas M. Smith<sup>†</sup> and S. Menon<sup>‡</sup>  
School of Aerospace Engineering  
Georgia Institute of Technology  
Atlanta, GA 30332-0150

## Abstract

A methodology for solving unsteady premixed turbulent flame propagation problems in high Reynolds number ( $Re$ ), high Damköhler number ( $Da$ ) spatially evolving flows is developed. The method is based on Large-Eddy Simulation (LES) with a subgrid combustion model based on the Linear-Eddy Model (Kerstein, 1991). An inter-LES cell burning mechanism has been added to the present formulation to account for molecular diffusion (burning) across LES cells which was been neglected in earlier studies. Two-dimensional simulations of passive isotropic flame propagation using the LES-LEM for  $Re$  from 100 to 1000 are conducted to validate the subgrid and supergrid propagation mechanisms. Two models are used to simulate turbulent premixed stagnation point flames. The first model is a conventional approach which uses a thin flame model (Kerstein *et al.*, 1988) with and without significant heat release. The second model uses the LES-LEM approach without heat release. Qualitative comparisons between simulations and experimental data are made.

## 1 Introduction

Numerical procedures for calculating turbulent reacting flows at high Reynolds numbers ( $Re$ ) encountered in engineering situations have been mainly limited to steady state Reynolds Averaged Navier-Stokes (RANS) approximations. In RANS, the effects of all turbulent scales on the mean quantities are modeled simultaneously, typically using gradient transport assumptions

to compute terms arising from Reynolds-averaging the governing equations. In some cases, probability density functions (pdf's) are used to describe the interactions between chemical reactions and turbulence. While quantities such as the mean fuel consumption rate and the mean heat release may be estimated by RANS, transient flame-turbulence interactions such as local extinction can not be captured in a steady state calculation. Therefore, the need still exists for a methodology that is capable of capturing transient and unsteady phenomena in turbulent reacting flows.

The difficulty in simulating unsteady combustion problems lies in the problem of resolving the enormous range of active scales encountered in high  $Re$  and high Damköhler numbers ( $Da$  is defined as the ratio of a characteristic flow time to a chemical time scale) reacting flows. In high  $Da$  flows chemical reactions occur in thin *sheets*. This increases the requirement for resolution far exceeding the requirement of resolving the turbulent scales alone. Since the flame interacts with turbulence at the smallest scales, the small scale interactions can not be neglected. Direct Numerical Simulation (DNS) is an ideal method from the standpoint that no closure models are required since all active scales are resolved on the computational grid. DNS of premixed freely propagating flames in isotropic turbulence (Trouvé and Poinso, 1994) and through isolated vortex pairs (Poinso *et al.*, 1991) have provided an increased understanding of flame-turbulence interactions including Lewis number effects and a mechanism for local extinction. Although it remains a valuable research tool, present and foreseeable computational capabilities restrict DNS to moderate  $Re$  and low  $Da$  flows.

Large Eddy Simulation (LES) is a promising technique that bridges the gap between the steady state assumption made by RANS and the intractable comprehensive DNS approach. In LES of turbulent non-

\*Copyright ©1997 by T. M. Smith and S. Menon. Published by the American Institute of Aeronautics and Astronautics, Inc., with permission.

<sup>†</sup>Graduate Research Assistant, Student Member, AIAA

<sup>‡</sup>Associate Professor, Senior Member, AIAA

reacting flows, the energy-containing large scales are directly simulated and the subgrid scales (assumed to be locally isotropic) are modeled.

Models based on the subgrid kinetic energy can be used (Kim and Menon, 1996) to compute the subgrid stress in the filtered equations. Turbulent flows may be simulated with adequate accuracy and at a fraction of the computational expense compared to DNS.

LES of turbulent reacting flows has received less attention mainly due to the lack of adequate subgrid combustion models. However, recent studies have proposed the adoption of the Linear Eddy Model (LEM) of Kerstein (1991,1992) (Menon *et al.*, 1994; Calhoun and Menon, 1996; 1997) as a subgrid combustion model. LEM is a stochastic mixing model that simulates scalar diffusion and turbulent mixing (convection) separately and accounts for all relevant scales of motion explicitly. For premixed flames, this means that the one-dimensional flame structure is resolved and all scales of flame wrinkling are explicitly captured by the model. The LES-LEM uncoupled approach has been demonstrated on transient premixed flame propagation in mixing layers (Menon *et al.*, 1994) and a coupled procedure has been developed for non-premixed reacting mixing layers (Calhoun and Menon, 1996; 1997).

This paper focuses on LES of premixed turbulent combustion with an emphasis on subgrid combustion modeling. To this end, a coupled LES-LEM procedure is developed for premixed turbulent combustion in the laminar flamelet regime and its specific application to stagnation point flows is discussed. Several issues unique to premixed combustion LES of turbulent stagnation point flames using a thin flame model with and without heat release are also presented.

The stagnation point flow has been chosen for several reasons. First, the flow field is stationary so the flame achieves a stationary position. A premixed turbulent jet impinging on a flat plate produces a diverging flow and a decelerating mean velocity. Therefore, a flame propagating upstream into the premixture and away from the plate will encounter an increasing velocity. As a result, a flame perturbed upstream will be convected back toward the plate while a flame perturbed downstream toward the plate will burn faster than the local fluid velocity and will propagate back upstream until a balance between flame speed and fluid velocity is reached. The stationary nature of the flame provides a convenient means for gathering statistical data necessary for evaluating the subgrid combustion model and for analyzing the properties of the flame. Along with stationary propagation, the flame propagates normal to

the impinging jet, a situation that simplifies modeling. In addition, an unambiguous turbulent flame speed can be defined. This configuration has been studied extensively experimentally (Cho *et al.*, 1986; Cho *et al.*, 1988; Liu and Lenzc, 1988; Shepherd *et al.*, 1990; Shepherd and Ashurst, 1992; Yahagi *et al.*, 1992) and, therefore, a database for comparison is available. Finally, the mean strain rate of the flow, and therefore, the flame surface (in the plane of the flame) strain rate can be controlled by systematically varying the mean jet inflow velocity. The effect of flame stretch (due to strain rate) on flame speed can then be systematically studied. Subgrid model response to a varying strain field will provide an important test of the model's capabilities.

The following section describes the LES numerical procedure and thin flame model followed by a description of LEM including recent developments and results from stand alone LEM calculations of freely propagating flames. These results demonstrate the potential of the LEM as a subgrid combustion model for premixed combustion in different regimes. The procedure for LEM as a subgrid combustion model is then discussed. Results from passive simulations of flame propagation in homogeneous turbulence at high  $Re$  are presented. The simulation of stagnation point flows using a conventional approach and the LES-LEM approach is then discussed followed by results from simulations and, finally, conclusions are made.

## 2 Model Formulation

A model for the computation of unsteady premixed combustion processes is presented in this section. The model is made up of the filtered equations of motion and supplementary sub-models for the propagation of reacting fronts.

### 2.1 LES Equations

In LES, the flow variables are decomposed into the resolved scale and the subgrid scale components. The large scales are computed explicitly while the effects of the subgrid scales on the large scales are modeled. The large scales contain most of the energy and the small scales primarily dissipate energy transferred from the large scales. Dynamics of large scale motion are dictated by the geometry of the flow field and the Reynolds number, while the small scale motion is relatively unaffected by the geometry except near walls. The subgrid length scales and times scales are small compared to

the large scales and, thus, the small scale motion adjusts faster and are considered more isotropic than the large scales. These concepts have been used to develop subgrid models.

Following Erlebacher *et al.* (1987), the flow variables are decomposed into the resolved scale and unresolved scale (subgrid scale) components by a spatial filtering operation such that  $f = \bar{f} + f''$ , where the  $(\sim)$  denotes resolved scale and the double prime ( $''$ ) denotes subgrid scale quantities. The Favre filtered variable is defined as  $\tilde{f} = \overline{\rho f} / \bar{\rho}$  where the overbar represents a spatial filtering which is defined as

$$\overline{\rho f(x_i, t)} = \int_D \rho f(z_i, t) F(x_i - z_i, \Delta) dz_i \quad (1)$$

$F$  is the filter kernel,  $D$  is the domain of the flow and  $\Delta$  is computational cell width in each spatial direction. The filtering operation is normalized by requiring that

$$\int_D F(x_i - z_i, \Delta) dz_i = 1. \quad (2)$$

It follows from eqs. (1) and (2) that for equally spaced and weakly stretched grids,  $\partial \bar{f} / \partial t = \partial f / \partial t$  and  $\partial \tilde{f} / \partial x_i = \partial f / \partial x_i$ . Filtering removes the high wave number range of Fourier components of the flow variables and separates the resolved scale components from the subgrid scales. In this study, a box filter is implicitly assumed which is appropriate for finite volume schemes. The filter function  $F$  takes on the values

$$F = \begin{cases} 1/\Delta^3 & -\frac{\Delta}{2} \leq (x_i - z_i) \leq \frac{\Delta}{2} \\ 0 & \text{otherwise.} \end{cases}$$

Contrary to the more traditional Favre temporal averaging,  $\tilde{f} \neq \bar{f}$  and, in general,  $\tilde{f}'' \neq 0$ . Applying filtering to the Navier-Stokes equations results in the following LES equations for a single component fluid (Smith and Menon, 1996a)

$$\frac{\partial \bar{\rho}}{\partial t} + \frac{\partial \bar{\rho} \tilde{u}_i}{\partial x_i} = 0 \quad (3)$$

$$\frac{\partial \bar{\rho} \tilde{u}_i}{\partial t} = \frac{\partial}{\partial x_j} [\bar{\rho} \tilde{u}_i \tilde{u}_j + \bar{p} \delta_{ij} - \bar{\tau}_{ij} + \tau_{ij}^{sgs}] = 0 \quad (4)$$

$$\frac{\partial \bar{\rho} \tilde{E}}{\partial t} + \frac{\partial}{\partial x_i} [(\bar{\rho} \tilde{E} + \bar{p}) \tilde{u}_i + \bar{q}_i - \tilde{u}_i \bar{\tau}_{ji} + H_i^{sgs} + \sigma_{ij}^{sgs}] = 0 \quad (5)$$

$$\tau_{ij} = \mu (\partial u_i / \partial x_j + \partial u_j / \partial x_i) - \frac{2}{3} \mu \partial u_k / \partial x_k \delta_{ij} \quad (6)$$

$$\bar{q}_i = -\bar{\kappa} \frac{\partial \tilde{T}}{\partial x_i}. \quad (7)$$

The subgrid closure terms are given by

$$\tau_{ij}^{sgs} = \bar{\rho} [\widetilde{u_i u_j} - \tilde{u}_i \tilde{u}_j] \quad (8)$$

$$H_i^{sgs} = \bar{\rho} [\widetilde{E u_j} - \tilde{E} \tilde{u}_j] + [\overline{p u_i} - \bar{p} \tilde{u}_i] \quad (9)$$

$$\sigma_{ij}^{sgs} = [\overline{u_j \tau_{ji}} - \tilde{u}_j \bar{\tau}_{ji}]. \quad (10)$$

In the above equations,  $\mu(T)$  is the molecular viscosity,  $\bar{\kappa} = c_p \mu / Pr$ ,  $Pr$  is the Prandtl number and  $c_p$  is the specific heat at constant pressure. Combustion is modeled using a thin flame model as discussed below. This eliminates the need to solve the filtered species equation as discussed later. The pressure is determined from the filtered equation of state,  $\bar{p} = \bar{\rho} R \tilde{T}$  where constant molecular weights and specific heats are assumed (assumptions that will be used in simulations discussed in the next section). The filtered total energy per unit volume is given by  $\bar{\rho} \tilde{E} = \bar{\rho} \tilde{e} + \frac{1}{2} \bar{\rho} \tilde{u}_i \tilde{u}_i + \frac{1}{2} \bar{\rho} [\widetilde{u_i u_i} - \tilde{u}_i \tilde{u}_i]$ , and the filtered internal energy is given by  $\tilde{e} = c_v \tilde{T} + h_f$ .

In order to solve this system of equations, the subgrid terms  $\tau_{ij}^{sgs}$ ,  $H_i^{sgs}$ , and  $\sigma_{ij}^{sgs}$  are replaced by models. In addition, it is necessary to obtain the subgrid turbulence intensity to couple the LEM (which is discussed below). Subgrid models for compressible flows are still relatively new (Erlebacher *et al.*, 1987; Squires and Zeman, 1990; and Moin *et al.*, 1991). In this study, we employ a compressible version of the dynamic one-equation model for the subgrid kinetic energy proposed by Kim and Menon (1996). This equation is given by

$$\frac{\partial \bar{\rho} k^{sgs}}{\partial t} + \frac{\partial}{\partial x_i} (\bar{\rho} \tilde{u}_i k^{sgs}) = P_{k^{sgs}} - D_{k^{sgs}} + \frac{\partial}{\partial x_i} (\bar{\rho} \nu_t \frac{\partial k^{sgs}}{\partial x_i}). \quad (11)$$

Here,  $k^{sgs} = \frac{1}{2} [\widetilde{u_i u_i} - \tilde{u}_i \tilde{u}_i]$  is the subgrid kinetic energy, and the subgrid turbulence intensity is related by  $u'_{sgs} = \sqrt{\frac{2}{3} k^{sgs}}$ . Note that  $u'_{sgs} \neq u''_i$  which represents the fluctuating part of  $u_i$ . The first and second terms on the right hand side of eq. (11) are the rates of production and dissipation of subgrid kinetic energy. In this model, the assumption that production and dissipation balance is not necessary. The formulation neglects the pressure dilatation term that appears in the original exact  $k^{sgs}$ -equation for two reasons. First, it is still unclear how to model the pressure dilatation in terms of the resolved flow field variables, and second, at low fluctuating Mach numbers, its influence may be negligible. The production is modeled as  $P_{k^{sgs}} = C_k \tau_{ij}^{sgs} \partial \tilde{u}_i / \partial x_j$  and the dissipation has the

form  $D_{k^{sgs}} = C_\epsilon \bar{\rho} (k^{sgs})^{3/2} / \Delta_g$  where  $\Delta_g$  is a characteristic grid size and  $\nu_t$  is the subgrid eddy viscosity given by  $\nu_t = C_\nu (k^{sgs})^{1/2} \Delta_g$ . The constants appearing in the above equations,  $C_k = 1.0$ , and  $C_\nu(x_i, t)$ ,  $C_\epsilon(x_i, t)$ , are solved dynamically (Kim and Menon, 1996).

The  $k^{sgs}$ -equation is solved simultaneously with the rest of the flow equations. With  $k^{sgs}$  and  $\nu_t$  determined, the subgrid shear stresses are evaluated as

$$\tau_{ij}^{sgs} = -2\bar{\rho}\nu_t(\tilde{S}_{ij} - \frac{1}{3}\tilde{S}_{\Pi}\delta_{ij}) + \frac{2}{3}\bar{\rho}k^{sgs}\delta_{ij} \quad (12)$$

where  $\tilde{S}_{ij} = \frac{1}{2}(\partial\tilde{u}_i/\partial x_j + \partial\tilde{u}_j/\partial x_i)$  is the resolved scale stress tensor. The subgrid energy flux is approximated as

$$H_i^{sgs} = -C_\epsilon\bar{\rho}\nu_t\frac{\partial\tilde{H}_i^{sgs}}{\partial x_i} \quad (13)$$

where  $\tilde{H}$  is the filtered total enthalpy,  $\tilde{H} = c_p\tilde{T} + \frac{1}{2}\tilde{u}_i\tilde{u}_i + k^{sgs} + h_f$ . The model constant,  $C_\epsilon = 1/Pr_t$  where  $Pr_t$  is the turbulent Prandtl number, is held constant. The subgrid closure term  $\sigma_{ij}^{sgs}$  and third order correlations arising as a result of this modeling approach have been neglected.

## 2.2 Thin Flame Propagation Model

In high  $Da$  premixed combustion fast chemistry results in very thin flame fronts. The thermo-diffusive character of a propagating thin flame remains unchanged by the turbulent flow and therefore can be modeled as a propagating front. To simulate premixed combustion as a propagating surface, the thin-flame model of Kerstein *et al.* (1988) is used in which a progress variable  $G$  is defined that evolves according to the equation

$$\frac{\partial G}{\partial t} = u_i \frac{\partial G}{\partial x_i} = u_f \left| \frac{\partial G}{\partial x_j} \right| + C_G \nu_t \frac{\partial^2 G}{\partial x_j \partial x_j} \quad (14)$$

where  $u_i$  is the fluid velocity and  $u_f$  is the local propagation speed. This equation is solved simultaneously with the LES equations. Equation (14) describes the convection of a level surface, defined as  $G = G_o$ , by the fluid velocity while simultaneously undergoing propagation normal to itself at a speed  $u_f$  according to Huygens' principle. In the flow field, the value of  $G$  is in the range  $[0,1]$  and in flame front modeling,  $G$  exhibits a step function like behavior, separating the burnt region ( $G < G_o$ ) from the unburned region ( $G > G_o$ ).  $G$  is assigned the value of unity in the unburned region and zero in the burnt region with the thin flame identified by a fixed value of  $0 < G_o < 1$ . In situations where zero heat release is assumed, any value of  $G =$

constant identifies a flame front. Thus, the physical interpretation is that an evolving  $G$ -level for any level  $G$  represents the simulated propagation of the constant property surface of that level. Furthermore, statistics from all values of  $G = \text{constant}$  can be combined; in effect, each simulation corresponding to a family of simulations parameterized by  $G$ .

In cases of non-zero heat release, the internal energy is now a function of  $G$ ,  $\tilde{e} = c_v\tilde{T} + h_f G$  where  $h_f = c_p(T_p - T_f)$  is a heat release parameter. In this case  $h_f$  should be a heavy side function of  $G$ , however, this produces a numerical instability when the flame front is steeply varying. Menon (1991) has pointed out that the linear dependence on  $G$  results in a distributed heat release that tracks the flame and does not cause significant error as long as the front is not a broad front.

The second term on the right hand side of eq. (14) does not appear in the original equation, however it was added here in order to avoid false minima from occurring in the flow. A false minima is not physically meaningful and results from a lack of resolution of the scalar field. Ashurst (1993) and Smith and Menon (1996a) added a similar term to eq. (14) for their simulations of propagating surfaces in isotropic turbulence. The constant  $C_G = 0.25$  was used in all simulations reported here. Analysis the simulation data showed that this term does not affect the key results of this study and furthermore that, in most of the simulated cases, less than 10% of the grid points exhibited this false minima.

In LES of premixed combustion,  $u_f$  is considered the turbulent flame speed  $u_t$  averaged over a characteristic volume. The turbulent flame speed is not known explicitly and must be modeled. We employ the RNG model of Yakhot (1988); an analytical expression for the turbulent flame speed as a function of turbulence intensity

$$u_t/S_L = \exp[(u'_{sgs})^2/(u_t)^2]. \quad (15)$$

Here,  $S_L$  is the unstretched planar laminar flame speed, and thus, the solution of the one-equation model for the subgrid kinetic energy provides the subgrid turbulence intensity necessary to close eq. (14). This equation was obtained by applying renormalization group theory to the  $G$ -field equation. The model assumes that the flame is a thin sheet having no internal structure and, therefore, it is applicable only in the flamelet combustion regime. The RNG model does not take into account  $Da$  or Karlovitz number ( $Ka$ ) effects and, therefore, can not predict extinction.

The laminar flame speed contains information about the chemical kinetics and molecular diffusion and, once the local subgrid turbulence intensity is determined, eq.

(15) can be used to determine  $u_f$  for a given fuel mixture. Equation (15) is a nonlinear equation and direct application requires the use of an iterative procedure. Therefore, to reduce computational cost, a look-up table is first generated and then  $u_f$  is linearly interpolated from the table in the simulations.

### 2.3 Linear-Eddy Model Applied to Premixed Combustion

In this section the Linear-Eddy model is developed for flamelet propagation through homogeneous turbulence. Recent results from stand-alone computations are included to show the model's capabilities to capture key flame-turbulence interactions. Modifications to include finite-rate and thermo-diffusive effects have been carried out in previous studies (Smith and Menon, 1996b; 1996c).

The LEM is used to fully characterize the effects of turbulent diffusion on the reaction-diffusion processes in the flame zone. To resolve all the length scales, the computational domain is restricted to one dimension which is considered to be a statistical ray through the local three-dimensional flame brush in the direction of mean propagation (Kerstein, 1986). The resolution within this one-dimensional domain is chosen to resolve all the relevant length scales ranging from the model integral length scale  $L$  to the smallest Kolmogorov eddy  $\eta$  or the laminar flame thickness,  $\delta_l$ , whichever is smaller.

LEM incorporates turbulent stirring (convection) and laminar propagation (reaction-diffusion) separately with no mass averaged velocity. In the LEM, convection is accomplished by instantaneous scalar field rearrangement events and cell volume expansion caused by heat release. These two mechanisms are discussed below. Physically, turbulent stirring increases the propagation rate by wrinkling (increasing) the flame surface while laminar burning acts to smooth (decrease) the flame surface.

The LEM relates fluid element diffusivity to a random walk of a marker particle. The total turbulent diffusion of a marker particle caused by eddies of size ranging from  $L$  to  $\eta$  based on *triplet mapping* (Kerstein, 1991) is given by

$$D_T \approx \nu(L/\eta)^{4/3} = \frac{2}{27} \lambda \int_{\eta}^L l^3 f(l) dl. \quad (16)$$

Turbulent stirring is modeled as stochastic rearrangement events which interrupt the deterministic flame propagation. Each rearrangement event is interpreted

as the action of a single eddy on the scalar field. Three quantities govern each event: the segment (eddy) size, the location, and the rate of events. The size is determined randomly from a pdf of eddy sizes

$$f(l) = \frac{5}{3} \frac{l^{-3/3}}{\eta^{-5/3} - L^{-5/3}} \quad (17)$$

in the range  $\eta < l < L$  (obtained from inertial range scaling; Kerstein, 1991). The event location is randomly chosen from a uniform distribution within the one-dimensional domain. The event rate (or frequency per unit length) is determined using an analogy between fluid dispersion in the one-dimensional domain and turbulent diffusivity (Kerstein, 1991),  $D_T = u' L / C_\lambda$ , where  $C_\lambda$  is a model constant. In earlier studies, all constants appearing in the above noted scaling relations were set to unity. However, for quantitative comparison with high  $Re$  experimental data, calibration of these constants is required. For example, to compare LEM predictions of scalar mixing with DNS in homogeneous isotropic turbulence, the event rate was rescaled by relating the LEM diffusivity to the large-eddy turnover time in the DNS (McMurtry *et al.*, 1993). A similar procedure is carried out in the present study.

The event rate is determined as  $E = \lambda X_{LEM}$ , where  $X_{LEM}$  is the length of the one-dimensional domain and  $\lambda$  is the event frequency per unit length having dimensions [ $L^{-1}T^{-1}$ ] which is determined from (Kerstein, 1991)

$$\lambda = \frac{54}{5} \frac{\nu Re}{C_\lambda L^3} \frac{[(L/\eta)^{5/3} - 1]}{[1 - (\eta/L)^{4/3}]}. \quad (18)$$

The time interval between events is then given as  $\Delta t_{stir} = 1/(\lambda X_{LEM})$ . Here, the Kolmogorov length scale is determined from the familiar inertial range scaling law  $\eta = N_\eta L Re^{-3/4}$  where  $N_\eta$  is an empirical constant.

Once the event size and location are determined and the time of the event is reached, the rearrangement event is implemented using triplet mapping (Kerstein, 1991). This mapping first creates three copies of the selected segment and then increases the spatial gradients of the copies by compressing them by a factor of three and reversing the middle copy. Finally, the original segment is replaced by the new *mapped* segment. Each mapping event requires at least six LEM cells so that on a discretized domain,  $\eta$  is resolved by six points. The mapping event has several attributes analogous to turbulent convection. First, it is known that the flame sheet surface normal vector aligns with the most compressive strain rate direction which is mimicked by the compressive nature of the triplet mapping.

Second, mapping increases the number of crossings of a single scalar value which may be interpreted as an increase in surface area caused by flame wrinkling. Finally, turbulent scaling laws built into the model cause the rate of strain and rate of growth of flame surface area to be of the correct order of magnitude (Kerstein, 1991). The ensemble of mapping events captures key mechanistic features of turbulent stirring despite the temporally discrete representation of a time continuous process. Furthermore, omission of flame surface displacement in the other two directions (since the present model is one-dimensional) has been shown to cause significant errors only at very low turbulence intensities where a single flame persists instead of multiple flames (Kerstein, 1986). Note that the component of vorticity in the direction normal to the flame surface does not create additional flame surface area nor does it wrinkle the flame. However, the other two components of vorticity will contribute to flame stretch, increasing the flame surface area, which are accounted for in this model.

For flamelet regime combustion ( $\delta_l \ll \eta$ ), using the  $G$ -field equation, a model for flamelet combustion using the linear-eddy approach is formulated (designated GLEM). GLEM models laminar burning by the propagation equation (Menon and Kerstein, 1992; Smith and Menon, 1996c)

$$\frac{\partial G}{\partial t} = S_L |\nabla G|. \quad (19)$$

This equation tracks the propagation of a single value of  $G$  between  $G_{fuel} \leq G_0 \leq G_{prod}$ , where  $G_{fuel} = 1$  and  $G_{prod} = 0$ .  $G_0$  is a prespecified level surface representing the location of the flame. Therefore, flame propagation is described by one scalar instead of  $N + 1$  (Menon and Kerstein, 1992). The flame speed  $S_L$  is also a prespecified constant which accounts for all of the physio-chemical properties of the mixture. Since LEM resolves even step like fronts, no dissipation mechanism is necessary to prevent false minima from occurring in contrast to eq. (14).

Since there is no mathematical description of expansion caused by heat release in eq. (19), expansion is implemented in terms of a physical interpretation of its effect on the  $G$ -field. Therefore, expansion is implemented by first prescribing a reference value  $G_{exp}$  that defines a transition from fuel to product. After each time step, each new cell value,  $G_i^{n+1}$ , is compared to the old value,  $G_i^n$ . If the reference value is crossed during that time step, all the heat is released, the cell value is set to  $G_{prod}$  and a number ( $N_{exp} - 1$ ) of new  $G_{prod}$  cells are added adjacent to the old cell. Here  $N_{exp}$  is the

nearest integer ratio of  $T_p/T_f$ , where  $T_p$  is the product temperature and  $T_f$  is the fuel temperature.

Results from a previous study (Smith and Menon, 1996c) are included here in order to demonstrate the capabilities of the model to capture key characteristics of flame-turbulence interactions in homogeneous flows. Propagation of a premixed flame through an isotropic turbulent field is simulated by solving eqs. (17-19) on an equally spaced discretized line.

In fig. 1a, the normalized turbulent flame speed predicted by GLEM and LEM (with a global finite-rate model) are compared to Yakhot's model predictions. LEM predictions of  $u_t/S_L$  agree well with the RNG prediction for the entire range in  $u'/S_L$ . Hollow symbols in fig. 1a represent individual realizations of the fan-stirred experiments and the dotted curve is the best fit to the data given by the authors (Abdel-Gayed *et al.* 1984). Although the LEM predictions show differences in both magnitude and shape compared to the dotted line, they are still well within the spread of the experimental data.

In fig. 1b, results from simulations of four different  $Re$  are presented. Finite-rate flames were simulated at four different turbulence intensities,  $u'$ . The normalized turbulent flame speed is plotted for constant  $Re$  against  $S_L/u'$ . The data shows agreement in the general trends seen by Abdel-Gayed *et al.* (1979) at low turbulence intensity. The curves seem to collapse as  $S_L/u'$  increases. However, as  $u'$  increases, the LEM flame  $u_t/S_L$  reaches a plateau and as  $u'$  increases further,  $u_t/S_L$  tends toward zero. This may be the result of flame stretch. As  $S_L$  decreases, the flame thickness generally increases, thus, as  $S_L/u'$  decreases, the ratio  $\delta_l/\eta$  increases and therefore,  $Ka$  increases. Even though in-the-plane strain rate and flame surface curvature are multi-dimensional effects, the LEM contains elements of flame stretch by the nature of the one-dimensional thermo-diffusive curvature effects and the compressive strain induced by triplet mapping.

## 2.4 Linear-Eddy Subgrid Combustion Model

In the two preceding sections, the LES and LEM where described separately. In the present section, the LEM subgrid combustion model for LES is described.

The LES numerical procedure solves the unsteady, two-dimensional compressible filtered Navier-Stokes equations, the  $k^{sgs}$  model, and the GLEM in the subgrid using a finite-volume scheme based on the unsplit explicit MacCormack predictor-corrector method. The

scheme is formally fourth-order accurate in space and second-order accurate in time (Gottlieb and Turkel, 1976). In addition, the viscous derivatives are fourth-order accurate. The solution of the filtered density, momentum, and total energy is marched time accurately on the acoustic time scale ( $\Delta t_{LES}$ ).

LEM numerical procedure involves three subgrid processes, flame propagation, stirring, and expansion. In each LES cell, the subgrid scalar  $G$  is discretized on a line. Equation (19) is marched simultaneously with the LES equations. The subgrid turbulence intensity is obtained from the subgrid kinetic energy  $u'_{sgs} = \sqrt{\frac{2}{3}k'_{sgs}}$ . From  $u'_{sgs}$ , a characteristic cell length,  $\Delta x_{LES}$  and the local viscosity, the stirring properties (event frequency per unit length and eddy length scale distribution) are obtained. Therefore, the evolution of the subgrid scalar  $G$  is coupled to the LES by the subgrid kinetic energy and temperature dependent kinematic viscosity. To prevent numerical diffusion from contaminating the turbulent diffusion, the subgrid  $G$  is required to propagate as a steep front. This is accomplished by requiring that the discrete time step in eq. (19) equal an integer multiple of the flame burning time,  $\Delta t_{sgs} = \Delta x_{LEM}/S_L$ . Therefore,  $G$  always takes on a step function 0 (burnt) or 1 (unburnt). The consequence of this discretization is that the subgrid process  $\Delta t_{sgs}$  is different from  $\Delta t_{LES}$ .

Large scale convection between two adjacent LES cells is handled by *splicing* subgrid cells from a donating LES cell to a receiving LES cell (Menon *et al.*, 1992; Calhoun and Menon, 1996). The splicing algorithm calculates the volume flux to be transferred across the LES cell interface (in a finite volume formulation) based on the resolved velocity and subgrid turbulence intensity ( $\tilde{u}_i + u'_{sgs}$ ), removes an equivalent number of LEM cells from the donor LES cell and adds them to the receiving LES cell. The rate of transfer is based on the convective time scale of the resolved velocity,  $\Delta t_{CON} = \min(\Delta x_{LES}/\tilde{u}_i + u'_{sgs})$ , (Calhoun and Menon, 1996). Spurious scalar diffusion can occur when a group of LEM cells are spliced from one cell and placed adjacent to cells in another LES cell. This is because the scalar may not be continuous at the interface. Calhoun has advocated the use of subgrid partitions to help eliminate this problem. In the present study partitions are also used. In addition to partitions, convecting scalar values of either 0 or 1 was found to greatly reduce spurious diffusion when the mean flow is not aligned with a grid direction. This issue becomes less important as  $Re_{sgs}$  increases and therefore, it is not known whether these partitions will be necessary

in high  $Re$  fully developed turbulent simulations.

In the above discussion of the LES, LEM, and splicing procedures, three discrete time scales have been defined for the overall LES-LEM solution procedure. Therefore, while the three procedures describe the time accurate evolution of flow quantities, each procedure is marched on a different time scale.

Heat release occurs in the subgrid. Heat release is a heavy side function of  $G$  as discussed in connection to the  $G$ -field equation flamelet model for LES. The subgrid pressure is assumed to be constant but varies from LES cell to cell. Therefore, a change in  $T^{sgs}$  results in a change in  $\rho^{sgs}$  through the equation of state and reverse coupling between LEM and LES is through the supplementary equations, filtered temperature, and density. This results in redundant filtered temperature and density in the supergrid. Further work is required to resolve this issue however some progress has been made by Calhoun and Menon (1997).

One aspect of the LES-LEM approach that has been neglected in the past is molecular diffusion (or laminar propagation) across adjacent LES cells. In high  $Re$  flows with negligible intermittency, this may be a good approximation, however, in flow situations where negligible turbulence intensity is encountered locally, this assumption will not hold and will halt the propagation of the flame altogether. For this reason, an inter-LES cell propagation model has been included in the present implementation. The inter-LES cell propagation model determines if a situation occurs where a fully burnt product cell is adjacent to a fuel cell. If this case exists, burning across the LES cell is initiated. From a discretized point of view, this preserves Huygen's principle of flame propagation without increasing the burning rate or adding to the spurious diffusion. The inter-LES cell propagation model is demonstrated for the simple case of one-dimensional flame propagation with a varying mean velocity. In fig. 2 a single flamelet is initially specified in one LES cell. The laminar flame speed is 0.5 m/s. The mean velocity varies from 0 m/s to 0.75 m/s. The average propagation rate is computed by integrating the instantaneous propagation rate which is determined from the change in  $G$  in the subgrid multiplied by  $\Delta x_{LEM}/\Delta t_{sgs}$ . This is plotted against the time for the flame to travel  $\Delta x_{LES}$ . In all three cases, a short transition period is experienced followed by relatively constant propagation. These flames have propagated 10  $\Delta x_{LES}$  and the speed has varied from  $S_L$  by less than 1%.

That completes the description of the LES-LEM procedure. The LES-LEM approach eliminates sev-

eral problems associated with conventional combustion model closures. First, the flame front in the subgrid is treated numerically as a discontinuity and is convected in the subgrid with no numerical diffusion. Compared to solving the filtered species equations, this represents true laminar flamelet propagation. Secondly, the subgrid eliminates the need to specify  $u_f$ , the turbulent flame speed, because it is now part of the solution.

### 3 Results and Discussion

#### 3.1 DNS and LES of Isotropic Turbulence

The  $k^{sgs}$  subgrid turbulence model was tested by comparing to DNS of two-dimensional isotropic turbulence (Case I in Herring *et al.*, 1974). Previous simulations (not shown) compared directly with data from their paper and almost identical results were reproduced. The DNS was carried out on a  $512 \times 512$  computational grid,  $2\pi \times 2\pi$  m in dimension. The initial  $Re$  based on the integral length scale was 383, the integral length was 0.314 m and the kinematic viscosity was  $1 \times 10^{-3} \text{ m}^2/\text{s}$ . The initial turbulence intensity was 0.1 m/s. The LES was initialized by filtering the DNS field onto a  $128 \times 128$  grid and the subgrid kinetic energy was obtained by direct filtering. Figure 3a shows the initial theoretical energy spectrum, along with results from four simulations on a log-log plot. The spectra were taken at roughly four large-eddy turnover times based on the initial large-eddy turnover time. The filtered DNS data, the LES with dynamic evaluation of coefficients, and LES with no subgrid turbulence model agree well with the DNS spectrum. Note that there is significant backward transfer of kinetic energy ( $\Sigma$ ) from the small scales to the large scales. This is characteristic of two-dimensional decaying isotropic turbulence. Therefore, it may be argued that a subgrid turbulence model is not necessary for two-dimensional LES of isotropic turbulence. Further evidence of this can be observed in fig. 3b. In this figure, the decay of kinetic energy and subgrid kinetic energy normalized by the initial values at time  $t=0$  s are plotted against the normalized time. While the filtered DNS kinetic energy, LES with dynamic evaluation, and LES with no subgrid model follow the decay quite well, the constant coefficient model LES is significantly different. The decay of  $k^{sgs}$  for the dynamic evaluation model and constant coefficient model are compared to the filtered DNS values. Note that  $k^{sgs}$  decays much more rapidly than  $\Sigma$  and there-

fore, any  $k^{sgs}$  in the initial field is rapidly diminished in these two-dimensional simulations. This has important implications to the subgrid combustion modeling. This means that  $k^{sgs}$  does not provide adequate subgrid turbulence intensity to model the interaction between subgrid stirring and flame propagation. Therefore, in the following results presented here, the subgrid turbulence intensity is prespecified and held constant throughout the domain and time.

#### 3.2 DNS and LES-LEM of Isotropic Flame Propagation

DNS of freely propagating flames in isotropic two-dimensional turbulence were performed on a  $2\pi \times 2\pi$  using  $400 \times 400$  cell computational grid to provide a comparison with  $G$ -field equation flamelet propagation. The DNS solves the Navier-Stokes equations and either a global finite-rate mechanism or the  $G$ -field equation flame model. Inflow and outflow boundary conditions were non-reflecting and the transverse boundaries were periodic. The finite-rate parameters and the turbulence parameters were similar to those used by Haworth and Poinso (1992). A single flame was initialized in the center of the domain. The  $Re$  based on the initial integral length scale was 0.416 m, the turbulence intensity was 0.1 m/s and the kinematic viscosity was  $5 \times 10^{-4} \text{ m}^2/\text{s}$ . The ratio  $u'/S_L$  was initially 6.3, and  $T_p/T_f = 4$ . Four snapshots from two simulations and two different times (normalized by the initial large-eddy turnover time,  $\tau = 1, 2$ ) are shown in figs. 4a-4d. In these figures, the  $G$ -field equation model is compared to the finite-rate flames. At one and even two  $\tau$ , the flames look very similar as does the post flame vorticity. These results demonstrate that if enough resolution is used, the  $G$ -field equation model can mimic more complex combustion models. In addition,  $G$ -field equation simulations also require significantly less computational effort compared to the finite-rate model simulations, for these simulations about 33% less.

LES-LEM simulations of passive (zero heat release) flames were conducted on a  $2\pi \times 2\pi$ ,  $96 \times 96$  computational grid. The ratio  $u'/S_L$  was varied by increasing the turbulence intensity from 0.01 m/s to 0.1 m/s while  $S_L$  was held constant. The  $Re$  based on the integral length scale varied from 100 to 1000. The integral length scale was 0.4125 m, and the kinematic viscosity was  $4.125 \times 10^{-5} \text{ m}^2/\text{s}$ . The subgrid Reynolds number  $Re_{sgs}$  was specified as 5% of the supergrid  $Re$  and all model coefficients were set to unity. All four boundaries were periodic. Two flames were initialized one integral

length apart in the center of the domain. Figure 5a and 5b are snapshots of the twin flames at two large-eddy turnover times for the case of  $u'/S_L = 1$  and 10. The filtered field representing the flame brush is resolved by only one or two LES cells. The resolved flame area is very similar in both simulations even though the  $u'/S_L = 10$  is burning much more rapidly.

To study the propagation mechanisms in the LES-LEM approach, three propagation speeds are defined. The first is  $A_F/A_L$ , the resolved scale area ratio. For this geometry,  $A_L$  is simply twice the width of the domain. In flamelet combustion, the area ratio is approximately the ratio of the turbulent to laminar flame speed. Since these are transient simulations and no steady area is achieved, we hesitate to call this ratio the turbulent flame speed, nevertheless, the relative magnitudes give a good indication of what effects the model and flow parameters are likely to have on the turbulent flame speed. The second propagation speed defined as the subgrid turbulent flame speed ( $u_{tsgs}/S_L$ ) is a global average of the ratio of the number of flame crossings to a single (laminar) flame crossing. The global average is taken over all LES cells containing at least one flame crossing. The third propagation speed is the global scalar consumption rate. It is defined as ( $S_G = \frac{\Delta x_{LEM}}{\Delta t_{sgs}} \sum_{i=1}^{IMAX} \sum_{j=1}^{JMAX} \Delta G$ ).  $S_G$  represents the global destruction of  $G$ . In figs. 6a, 6b and 6c the three propagation rates are shown for the three isotropic simulations. The time axis is normalized by the initial large-eddy turnover time. In fig. 6a  $A_F/A_L$  is nearly constant for all three cases for just over two large-eddy turnover times and then the higher  $u'/S_L$  case burns out quickly. In fig. 6b the subgrid  $u_{tsgs}/S_L$  scales with  $Re_{sgs}$ . This can be explained as an increase in flame crossings due to more frequent stirring events taking place in the high  $u'/S_L$  case. In fig. 6c the average global consumption rate is plotted. This speed has been averaged in time. Again the consumption rate scales with  $u'/S_L$ .

### 3.3 Turbulent Stagnation Point Flames

#### 3.3.1 Geometric Configurations

Two geometric configurations were chosen to simulate turbulent stagnation point flames. The first was a rectangular geometry with a flat surface and the second was a rectangular geometry with a circular arc hump similar to the curved wall in the experimental apparatus of Cho *et al.* (1986). The computational domain is tilted 90 degrees to that of the experimental appa-

paratus so the flow is from left to right, the wall is along the vertical direction and the outflow boundaries are normal to the  $y$  direction. The wall was placed 0.075 m away from a 0.50 m diameter turbulent jet exit. In the experiments, a 0.2 m diameter co-flowing jet surrounds the turbulent jet in order to prevent large scale entrainment from the ambient air. Turbulence is generated by passing the premixed stream through a grid just prior to the converging nozzle. This produces a nearly uniform homogeneous turbulent stream.

To simulate a turbulent stagnation point flow, pseudo-turbulence is generated with a specified energy spectrum, turbulence intensity, and divergence free velocity field. A procedure similar to Lee *et al.* (1992) is used. The pseudo-turbulence is convected into the computational domain at the mean velocity. In addition, the random field is recomputed on a random time scale using random phase angles from a chosen wave number shell. For a given flow through time (based on the jet width and mean inflow velocity), each wave number shell is recomputed once. This prevents the inflow from becoming periodic while preventing significant discontinuities in the velocity field.

The turbulent jet is cropped near the boundaries using a cosine function raised to the power 0.95. This numerically simulates the uniform turbulent inflow and prevents a discontinuous inflow velocity at the interface between the turbulent jet and the outer co-flowing jet. The computational co-flowing jet extends to the edge of the outflow boundary to prevent entrainment at the inflow, a situation that is very difficult to handle from a computational point of view.

The computational boundaries normal to the inflow boundaries are extended past the plate diameter which is 0.2 m in order to damp oscillations in flow variables by means of grid stretching and filtering (Colonius *et al.*, 1993). Filtering is a convenient way to damp oscillations impinging on a computational boundary. The filter function is

$$\hat{f} = a(y)f_j + b(y)(f_{j+1} - f_{j-1}) + c(y)(f_{j+2} - f_{j-2}) \quad (20)$$

and the coefficients  $a(y)$ ,  $b(y)$ , and  $c(y)$  take the values 1, 0, and 0 respectively at the location where filtering begins in the physical region and become 5/8, 1/4, and -1/12 near the outflow boundary. Second order filtering is used at the cell next to the boundary. The coefficient functions are based on a simple linear function using the grid spacing

$$a(y) = \frac{5}{8} + \frac{3}{8}(\Delta y_j / \Delta y) \quad (21)$$

$$b(y) = \frac{2}{3}(1 - a(y)) \quad (22)$$

$$c(y) = \frac{1}{6}(a(y) - 1) \quad (23)$$

where  $\Delta y_f$  is the location where filtering begins and  $\Delta y$  is the local grid spacing in the  $y$  direction. In all simulations, filtering begins at a location outside the physical domain of interest; in this case the turbulent jet width.

### 3.3.2 Boundary Conditions

At an inflow boundary where a time varying velocity field is introduced, the velocity field and the temperature are prescribed and a characteristic boundary condition is normally used to solve for the density. Pressure is obtained through the equation of state (Poinsot and Lele, 1992). However, these boundary conditions were found to exhibit unstable pressure oscillations and so non-reflecting characteristic boundary conditions were used, modified from Menon and Jou (1990). In this case the stagnation pressure and temperature are prescribed functions of the  $y$ -coordinate and time, the  $v$ -component of velocity is also prescribed and the  $u$ -component is computed from the two-dimensional euler equations written in characteristic form and setting the magnitude of the incoming waves to zero. This set of boundary conditions greatly reduce the amplitude of the reflected pressure waves while allowing for the specification of an unsteady velocity inflow field. It should be noted that the specification of an unsteady velocity field results in a small unsteady velocity divergence and this divergence tends to increase with increasing inflow Mach number.

Non-reflecting characteristic boundary conditions are imposed on the vertical outflow boundaries similar to those suggested by Poinsot and Lele (1992). The wall is assumed to be no-slip and adiabatic.

### 3.3.3 LES with the G-Field Equation Model

Preliminary simulations of the stagnation point flow field and flame propagation have been made using the  $G$ -field equation flamelet model. For these conventional simulations, the flame speed is assumed constant and the geometry with a curved plate is used to match the experiments. Four simulations were conducted using a grid resolution of 97 x 129. Two cold-flow simulations used a computational domain width of 0.3 m and the two cases with heat release used a computational domain width of 0.5 m. It was necessary to increase

the computational domain for heat release cases because of interaction between out-flow boundary conditions and small amplitude pressure oscillations arising from unsteady heat release. The first two cases are for  $u'/S_L = 1.33$  and were conducted with and without heat release. The temperature ratios were  $T_p/T_f = 0, 4$  and the inflow Mach number based on the mean velocity ( $\bar{U} = 5.0$  m/s) was 0.1. The turbulent jet width consisted of 48 points,  $u' = 0.4$  m/s the integral length scale in the turbulent jet was 0.0037 m and  $Re = 80$ . In the second two cases,  $u'/S_L = 1.0$  and  $T_p/T_f = 0, 7$ . Snapshots of two simulations are shown in figs. 7a and 7b. The vorticity and flame contours are shown for  $u'/S_L = 1.0$  and  $T_p/T_f = 0, 7$ . The cold flow case shows larger scale wrinkling and a thinner flame front than the heat release case. It is also apparent from these figures that the hot flame interacts with the boundary layer. There is a tendency for the hot flame to be pushed closer to the wall. This effect is shown in fig. 8a which shows the mean axial location of the four flames. Statistics were collected for at least 5 flow through times after a stationary state was reached. This trend was not noticed in experiments. The r.m.s. velocity components in the axial direction are shown in figs. 8b and 8c. Data from experiments under similar conditions show nearly constant  $u'$  and  $v'$  in the axial direction and  $u' \approx v' \approx 0.2$  m/s in the region from 0.045 m to 0.07 m for the non-reacting case and an increase in  $u'$  in the flame region of the reacting case and an increase in  $v'$  in the reacting case very near the wall. Our data for this region show that  $u'$  slightly increases as well as  $v'$ . This is more pronounced in the reacting cases.

The mean axial velocity (not shown) is linear for the cold flow cases and show modest *humps* for the two heat release cases where an acceleration due to gas expansion occurs. The turbulent flame speed is estimated by the value of the mean axial velocity where the mean scalar is 0.95. In the experiments (Cho *et al.*, 1986) for a range in  $u_i/S_L$  from 1 to 2,  $u_i/S_L$  ranges between 2 to 3. Our  $u_i/S_L$  ranges between 1.275 to 2.45 for  $u'/S_L = 1, 1.33$ .

### 3.3.4 LES-LEM Model

Preliminary results from LES-LEM simulations are presented here. The stagnation wall is flat for these cases. Two simulations are conducted to demonstrate the feasibility of performing this type of calculation. Both simulations assume zero heat release, an assumption that will be relaxed in the near future and reported subsequently. The grid was 97 x 97, the distance from

nozzle exit to wall was again 0.075 m, the width of the computational domain was 0.3 m and  $\bar{U}=5$  m/s. The two simulations differ by  $u'/S_L = 1, 2$ ,  $Re = 80, 160$ , and  $Re_{sgs} = 19, 38$ . The subgrid time scale parameter was set equal to the value used by Calhoon and Menon, (1996). A snapshot of the vorticity and filtered  $G$  contours are shown in fig. 9a for  $u'/S_L = 2$ . The flame brush is highly convoluted by the relatively large turbulent structures present in the flow. Since the physical domain of interest is roughly the jet width, the LEM subgrid procedure is conducted only in a subdomain near the stagnation point. In these zero heat release simulations, the subgrid evolution is passive and it is convenient and efficient to solve for the evolution of the flame brush in this manner. Nearly stationary propagation rate data for the two simulations are presented in fig. 9b. Though it is obvious that more data is necessary to estimate mean quantities, it is also apparent that the burning rates are steady. Just as in the isotropic simulations, the propagation rates scale with the  $u'/S_L$ .

Though the results are only preliminary, they demonstrate that the LES-LEM procedure has the potential for turbulent flame propagation simulations.

## 4 Conclusions

A methodology for solving unsteady premixed turbulent flame propagation problems in high Reynolds number ( $Re$ ), high Damköhler number ( $Da$ ) spatially evolving flows has been developed for combustion in the laminar flamelet regime. The model can easily be modified to include finite-rate and thermo-diffusive effects (Smith and Menon, 1996b; 1996c). The method is based on LES with a subgrid combustion model based on the LEM (Kerstein, 1991). An inter-LES cell burning mechanism has been added to the present formulation to account for molecular diffusion (burning) across LES cells, a mechanism previously neglected. Passive isotropic flame propagation simulations using the LES-LEM for  $Re$  from 100 to 1000 were conducted to validate the subgrid and supergrid propagation mechanisms. Results show that the subgrid and supergrid burning rates scale with  $u'/S_L$  and  $Re$ . In addition, the filtered scalar that propagates as a steep front is resolved in these high  $Re$  flows with as little as one or two LES grid cells and subgrid flames are resolved by a single LEM cell width, reducing the numerical diffusion in the subgrid combustion processes. Two models were used to simulate turbulent premixed stagna-

tion point flames. The first model is a conventional approach which uses a thin flame model (Kerstein *et al.*, 1988) with and without significant heat release ( $T_p/T_f = 0, 4, 7$ ). The second model uses the LES-LEM approach without heat release. Qualitative comparisons between simulations and experimental data were made. Turbulent cold flow statistics and turbulent flame speeds agree reasonably well with experiments by Cho *et al.*, (1986), however reacting flow statistics deviate in magnitude. It is believed that the differences are caused by physical boundaries in the simulation differing from the experimental apparatus, in order to make the simulations possible.

Preliminary results for the stagnation point flame using the LES-LEM approach demonstrate that the application of LES-LEM to spatially evolving flows with complex mean fluid flow is feasible, stationary flame position and stationary burning rates are achieved, and that they scale properly with  $u'/S_L$ . Further work is needed for the specification of  $k^{sgs}$  in two-dimensional simulations.

## Acknowledgments

This work was supported in part by the Air Force Office of Scientific Research under the Focused Research Initiative, monitored by General Electric Aircraft Engines, Cincinnati, Ohio. Support for the computations was provided by the Army Research Laboratory, Aberdeen, Maryland and is gratefully acknowledged.

## References

- Abdel-Gayed, R. G., Bradley, D., and McMahon, M. (1979) "Turbulent Flame Propagation in Premixed Gases: Theory and Experiment," *Seventeenth Symposium (International) on Combustion*, The Combustion Institute, Pittsburgh, pp. 245-254.
- Abdel-Gayed, R. G., Al-Khishali, K. J. and Bradley, D. (1984) "Turbulent Burning Velocities and Flame Straining in Explosions," *Proc. R. Soc. Lond.*, A Vol. 39, pp. 393-414.
- Calhoon, W. H. and Menon, S. (1996) "Subgrid Modeling for Reacting Large Eddy Simulations," Presented at the 34th Aerospace Sciences Meeting, Reno, NV, January 15-18 AIAA-96-0516.

- Calhoon, W. H. and Menon, S. (1997) "Linear-Eddy Subgrid Model for Reacting Large-Eddy Simulations: Heat Release Effects," Presented at the 35th Aerospace Sciences Meeting, Reno, Nv, January 6-9 AIAA-97-0368.
- Cho, P., Law, C. K., Hertzberg, J. R., and Cheng, R. K. (1986) "Structure and Propagation of Turbulent Premixed Flames Stabilized in a Stagnation Flow," *Twenty-first Symposium (International) on Combustion*, The Combustion Institute, Pittsburgh, pp. 1493-1499.
- Cho, P., Law, C. K., Cheng, R. K., and Shepherd, I. G. (1988) "Velocity and Scalar Fields of Turbulent Premixed Flames in Stagnation Flow," *Twenty-Second Symposium (International) on Combustion*, The Combustion Institute, Pittsburgh, pp. 739-745.
- Colonus, T., Lele, S. K., and Moin, P. (1993) "Boundary Conditions for Direct Computation of Aerodynamic Sound Generation," *AIAA J.*, Vol. 31, No. 9, pp. 1574-1582.
- Erlebacher, G. Hussaini, M.Y. Speziale, C.G. and Zang, T.A. (1987) "Toward the Large-Eddy Simulation of Compressible Turbulent Flows," Institute for Computer Applications in Science and Engineering, Hampton, VA, ICASE 87-20.
- Gottlieb, D. and Turkel, E. (1976) "Dissipative Two-Four Methods for Time-Dependent Problems," *Math. of Comp.*, Vol. 30, No. 136, pp.703-723.
- Haworth, D. C. and Poinso, T. J. (1992) "Numerical Simulations of Lewis Number Effects in Turbulent Premixed Flames," *J. Fluid Mech.*, Vol. 244, pp. 405-436.
- Herring, J. R., Orszag, S. A., Kraichnan, R. H. and Fox, D. G. (1974) "Decay of Two-Dimensional Homogeneous Turbulence," *J. Fluid Mech.*, Vol. 66, pp. 417-444.
- Kerstein, A. R. (1986) "Pair-Exchange Model of Turbulent Premixed Flame Propagation," *Twenty-first Symposium (International) on Combustion*, The Combustion Institute, Pittsburgh, pp. 1281-1289.
- Kerstein, A.R., Ashurst, W.T., and Williams, F.A. (1988), "The Field Equation for Interface Propagation in an Unsteady Homogeneous Flow field", *Phys. Rev. A*. Vol. 37, pp. 2728.
- Kerstein, A. R. (1991) "Linear-Eddy Modeling of Turbulent Transport. Part 6. Microstructure of Diffusive Scalar Mixing Fields," *J. Fluid Mech.*, Vol. 231, pp. 361-394.
- Kerstein, A. R. (1992) "Linear-Eddy Modeling of Turbulent Transport. Part 4. Diffusion-Flame Structure and Nitric Oxide Production," *Combust. Sci. Tech.*, Vol. 81, pp. 75-86.
- Kim, W.-W. and Menon, S. (1996) "On the properties of a localized dynamic subgrid-model for large-eddy simulations," *Submitted to J. Fluid Mech.*
- Lee, S., Lele, S. K., and Moin, P. (1992) "Simulation of spatially evolving turbulence and the applicability of Taylor's Hypothesis in compressible flow," *Phys. of Fluids A*, Vol. 4, pp. 1521-1530.
- Liu, Y., and Lenze, B. (1988) "The Influence of Turbulence on the Burning Velocity of Premixed  $CH_4 - H_2$  Flames with Different Laminar Burning Velocities," *Twenty-Second Symposium (International) on Combustion*, The Combustion Institute, Pittsburgh, pp. 747-754.
- McMurtry, P. A. Gansauge, T. C., Kerstein, A. R., and Krueger, S. K. (1993) "Linear-Eddy Simulations of Mixing in a Homogeneous turbulent Flow," *Phys. Fluids A*, Vol. 5 pp. 1023-1034.
- Menon, S., and Jou, W.-H. (1990) "Numerical Simulations of Oscillatory Cold Flows in an Axisymmetric Ramjet combustor," *Journal of Propulsion and Power*, Vol. 6, No. 5, pp. 525-534.
- Menon, S. (1991) "Active Control of Combustion Instability in a Ramjet Using Large-Eddy Simulations," AIAA-91-0411, 29th Aerospace Sciences Meeting, Reno, Nv, January 7-10.
- Menon, S. and Kerstein, A. R. (1992) "Stochastic Simulation of the Structure and Propagation Rate of Turbulent Premixed Flames," *Twenty-Fourth Symposium (International) on Combustion*, The Combustion Institute, Pittsburgh, pp. 443-450.
- Menon, S., McMurtry, P. A. and Kerstein, A. R.

- (1994) "A Linear Eddy Subgrid Model for Turbulent Combustion: Application to Premixed Combustion," Presented at the 31st Aerospace Sciences Meeting, Reno, Nv, January 11-14, AIAA-93-0107.
- Moin, P., Squires, K., Cabot, W., and Lee, S. (1991) "A Dynamic Subgrid-Scale Model for Compressible Turbulence and Scalar Transport," *Phys. Fluids A*, No. 3, Vol. 11.
- Poinsot, T., Veynante, D. and Candel, S. (1991) "Quenching Processes and Premixed Turbulent Diagrams," *J. Fluid Mech.*, Vol. 228 pp. 561-606.
- Poinsot, T, J., and Lele, S. K. (1992) "Boundary Conditions for Direct Simulation of Compressible Viscous Flows," *J. Comp. Phys.*, Vol. 101 pp. 104-129.
- Shepherd, I. G., Cheng, R. K., and Goix, P. J. (1990) "The Spatial Scalar Structure of Premixed Turbulent Stagnation Point Flames," *Twenty-Third Symposium (International) on Combustion*, The Combustion Institute, Pittsburgh, pp. 781-787.
- Shepherd, I. G., and Ashurst, Wm. T. (1992) "Flame Front Geometry in Premixed Turbulent Flames," *Twenty-Fourth Symposium (International) on Combustion*, The Combustion Institute, Pittsburgh, pp. 485-491.
- Smith, T. and Menon, S. (1996a) "The Structure of Premixed Flames in a Spatially Evolving Turbulent Flow," *Combust. Sci. Tech.*, Vol. 119, No. 1-6.
- Smith, T. and Menon, S. (1996b) "Model Simulations of Freely Propagating Turbulent Premixed Flames," presented at the *Twenty-sixth Symposium (International) on Combustion*, The Combustion Institute, Pittsburgh.
- Smith, T. and Menon, S. (1996c) "One-Dimensional Simulations of Freely Propagating Turbulent Premixed Flames," *Submitted to Combust. Sci. Tech.*, September.
- Squires, K. and Zeman, O. (1990) "On the Subgrid-Scale Modeling of Compressible Turbulence," *Center for Turbulence Research, Proceedings of the Summer Program*.
- Trouve, A. and Poinsot, T. (1994) "The Evolution Equation for the Flame Surface Density in Turbulent Premixed Combustion," *J. Fluid Mech.*, Vol. 278, pp. 1-31.
- Yahagi, Y., Ueda, T., and Mizomoto, M. (1992) "Extinction Mechanism of Lean Methane/Air Turbulent Premixed Flame in a Stagnation Point Flow," *Twenty-Fourth Symposium (International) on Combustion*, The Combustion Institute, Pittsburgh, pp. 537-542.
- Yakhot, V. (1988) "Propagation Velocity of Premixed Turbulent Flames," *Combust. Sci. Tech.*, Vol. 60, pp. 9-24.

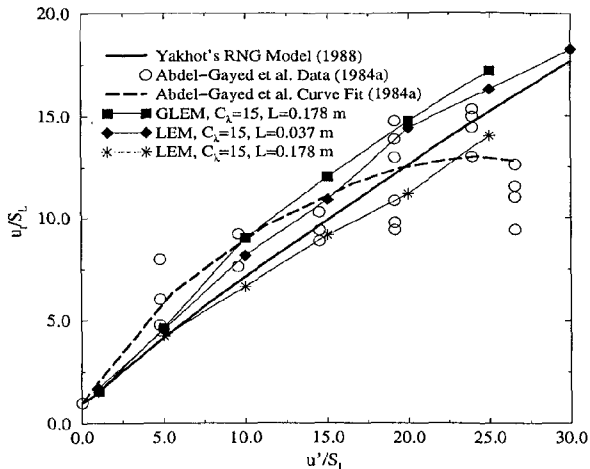


Fig. 1a Normalized turbulence flame speed for GLEM, and finite-rate LEM compared with Yakhot's model and the fan stirred bomb experiments of Abdel-Gayed et al. (1984).

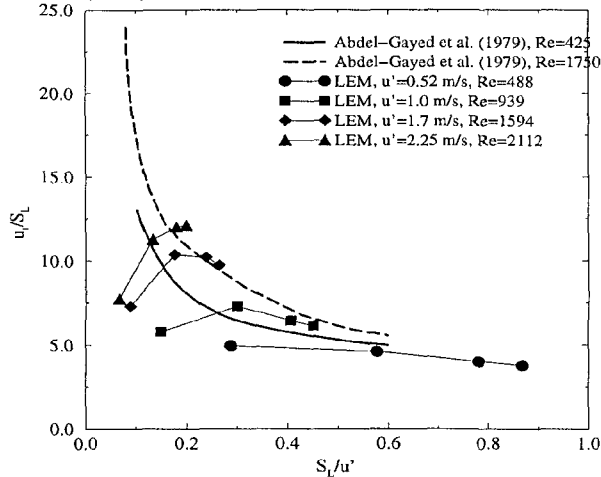


Fig. 1b Normalized turbulent flame speed as a function of normalized laminar flame speed for finite rate flames for different  $Re$  compared with the fan stirred bomb experiments of Abdel-Gayed et al. (1979).

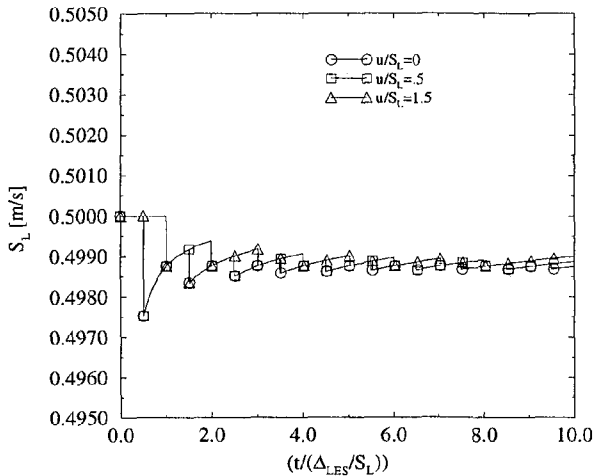


Fig. 2 One-dimensional inter-LES cell flame propagation.

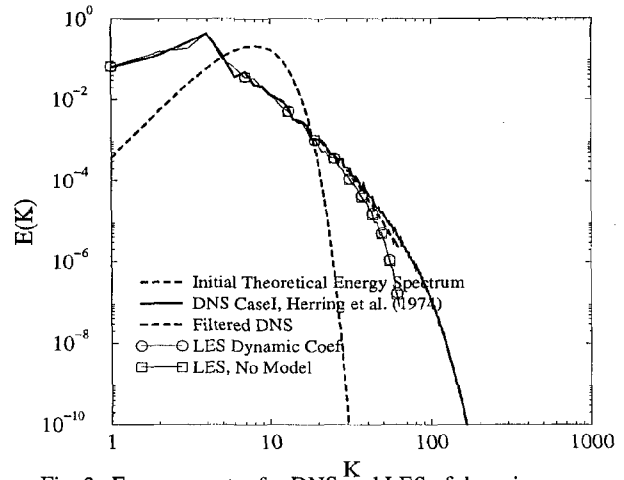


Fig. 3a Energy spectra for DNS and LES of decaying isotropic turbulence taken at  $\tau=4$ .

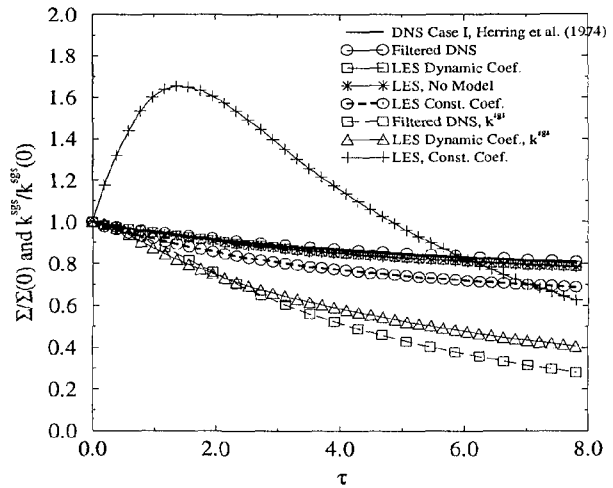
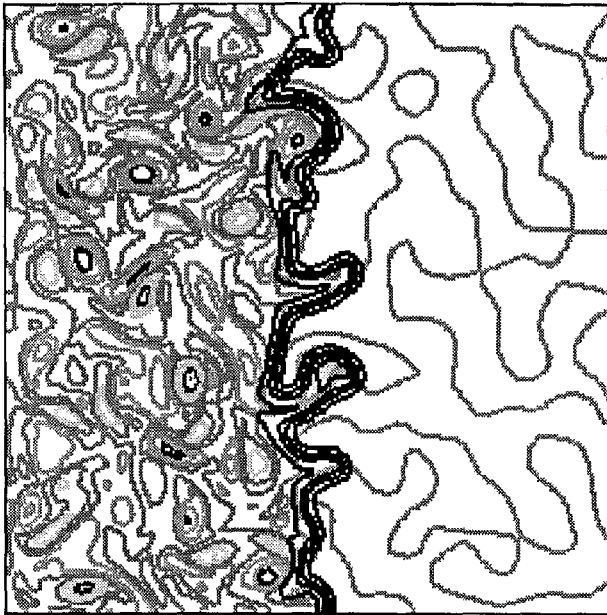
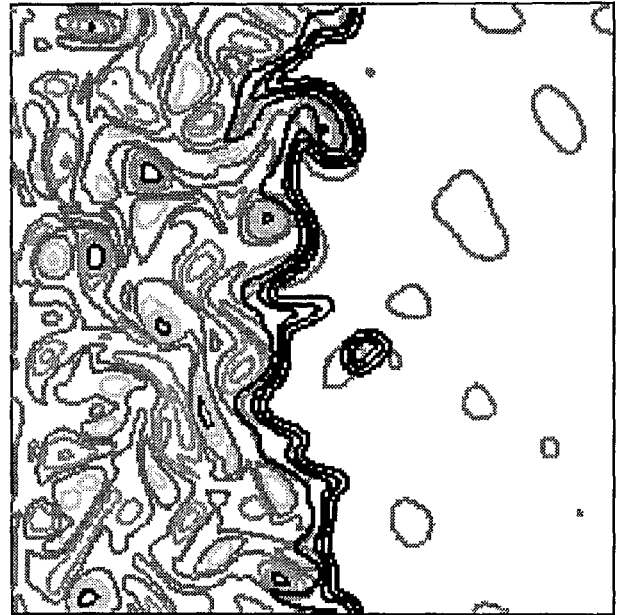


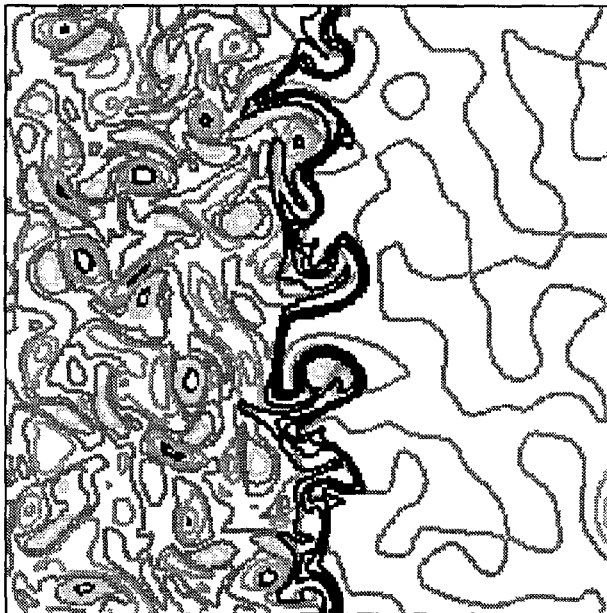
Fig. 3b Evolution of kinetic energy and subgrid kinetic energy.



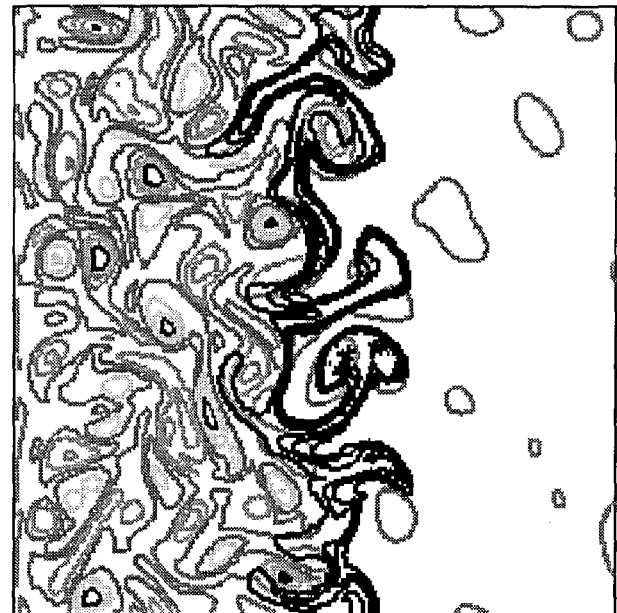
(a)



(b)



(c)



(d)

Fig. 4 DNS of freely propagating premixed flames in homogeneous turbulence. The evolution of species mass fraction from a global finite-rate combustion model is compared with the  $G$ -field equation. Snapshots of vorticity and a) mass fraction at  $\tau=1$ , b) mass fraction at  $\tau=2$ , c)  $G$ -field at  $\tau=1$ , and d)  $G$ -field at  $\tau=2$ .

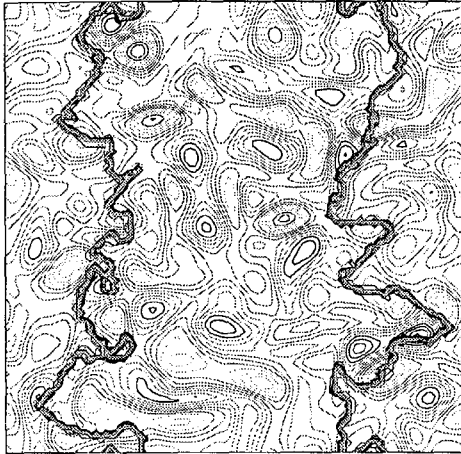


Fig.5a Snapshot of vorticity and filtered scalar from LES-LEM of passive flame propagation in decaying isotropic turbulence for  $u'/S_L=1.0$  and  $\tau=2$ .

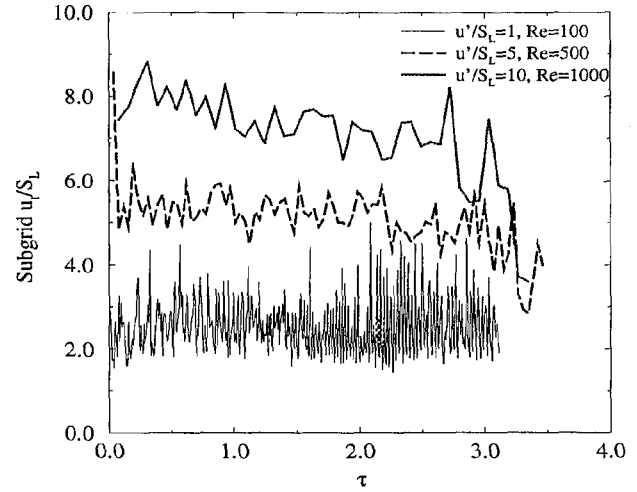


Fig.6b Evolution of normalized subgrid turbulent flame speed.

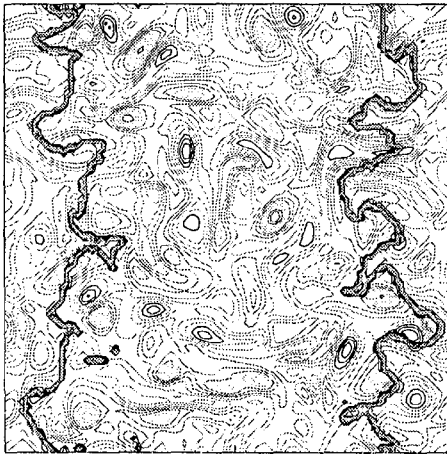


Fig.5b Snapshot of vorticity and filtered scalar from LES-LEM of passive flame propagation in decaying isotropic turbulence for  $u'/S_L=10.0$  and  $\tau=2$ .

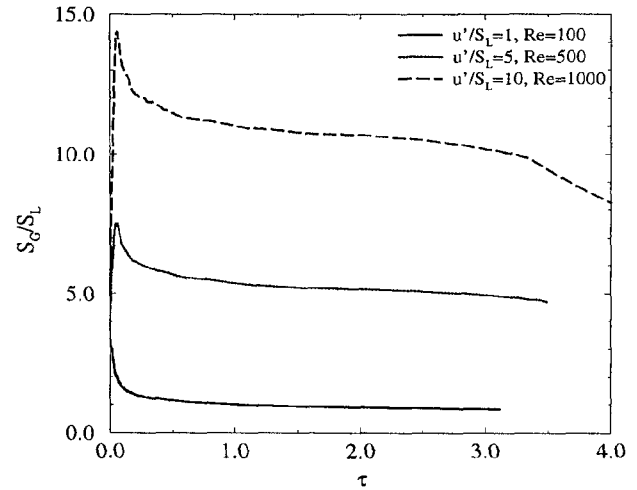


Fig.6c Evolution of normalized average scalar consumption rate.

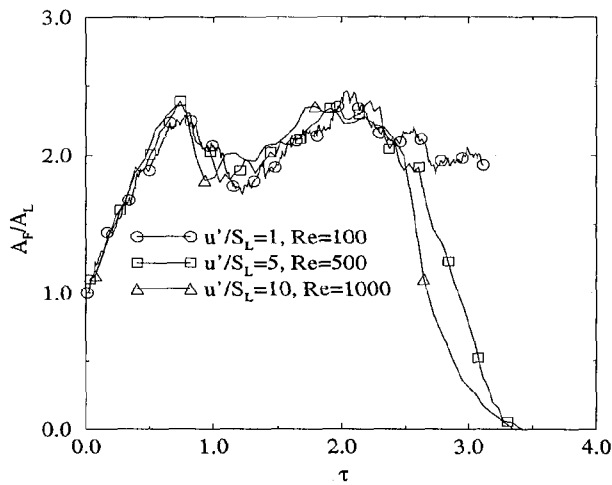


Fig.6a Evolution of normalized resolved flame area.

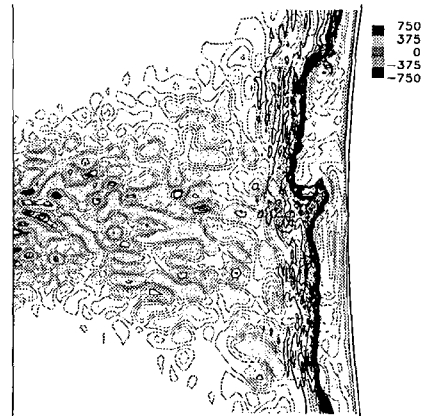


Fig.7a Snapshot of vorticity and  $G$ -field from cold flow stagnation point flame simulation.

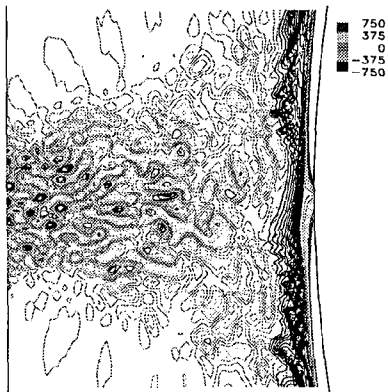


Fig.7b. Snapshot of vorticity and  $G$ -field from reacting flow stagnation point flame simulation.

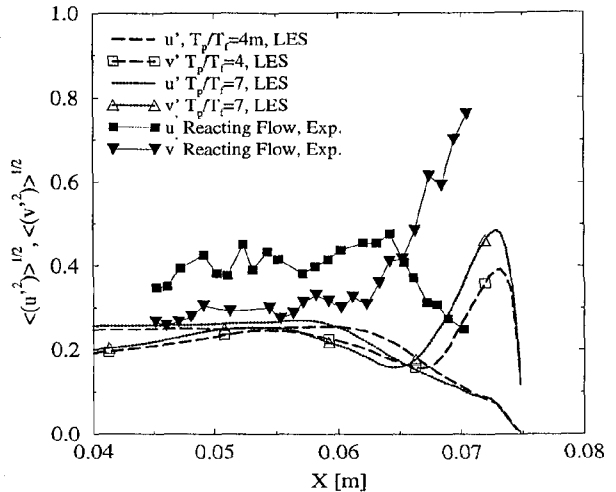


Fig.8c R.M.S. turbulence intensities for reacting flow stagnation point flames.

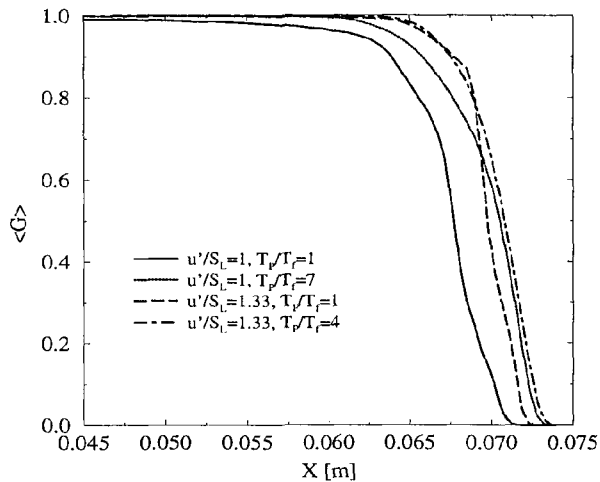


Fig.8a Mean axial flame locations.

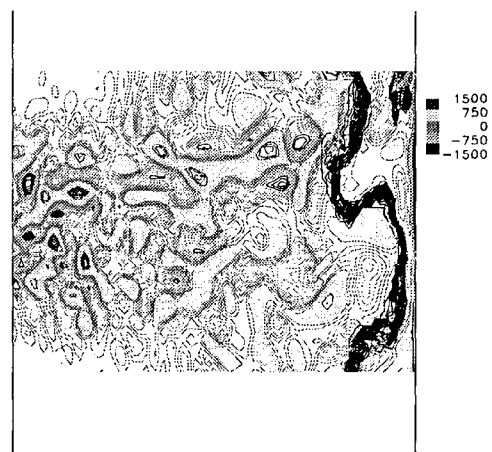


Fig.9a Snapshot of vorticity and the filtered scalar field from LES-LEM stagnation point flame.

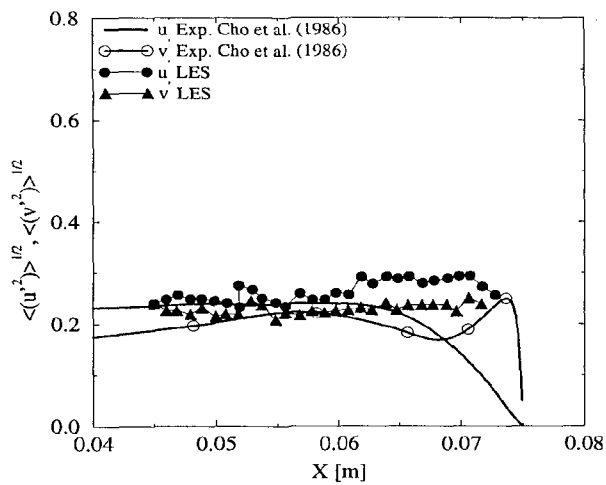


Fig.8b R.M.S. turbulence intensities for cold flow stagnation point flames.

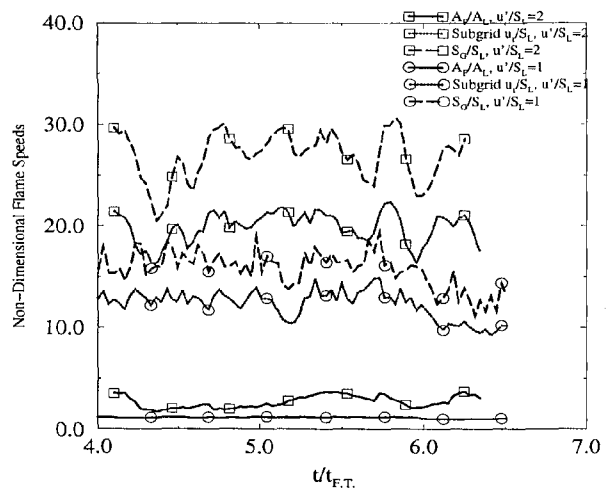
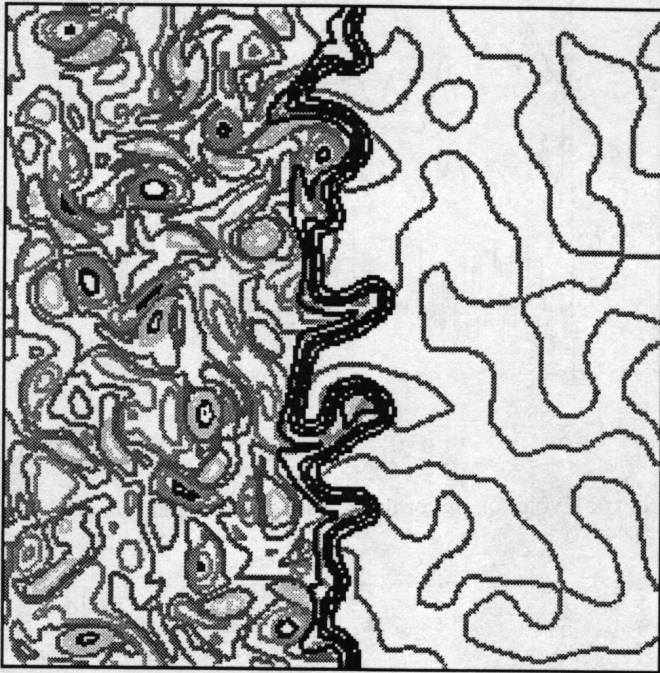
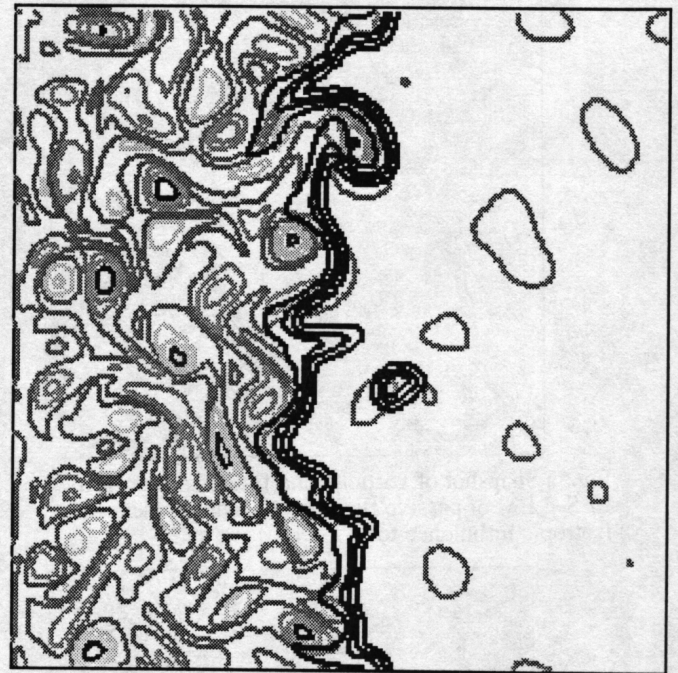


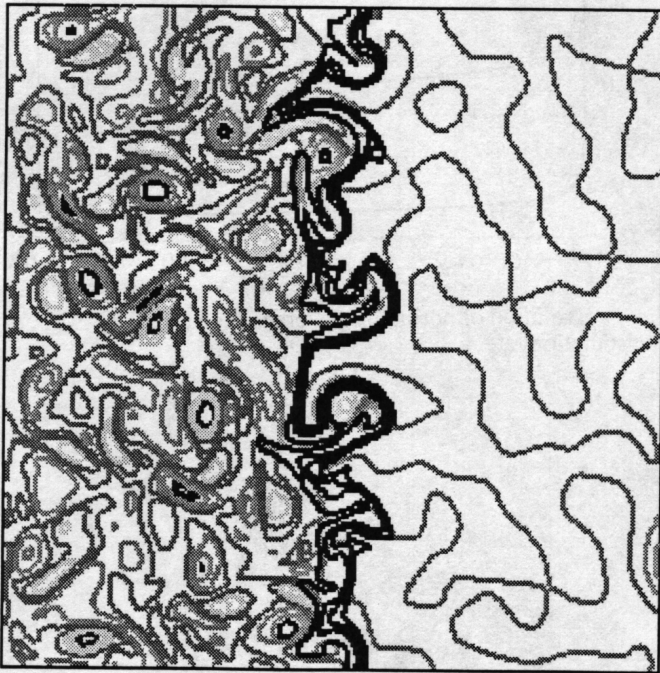
Fig.9b Evolution of propagation rates from LES-LEM simulation of stagnation point flame.



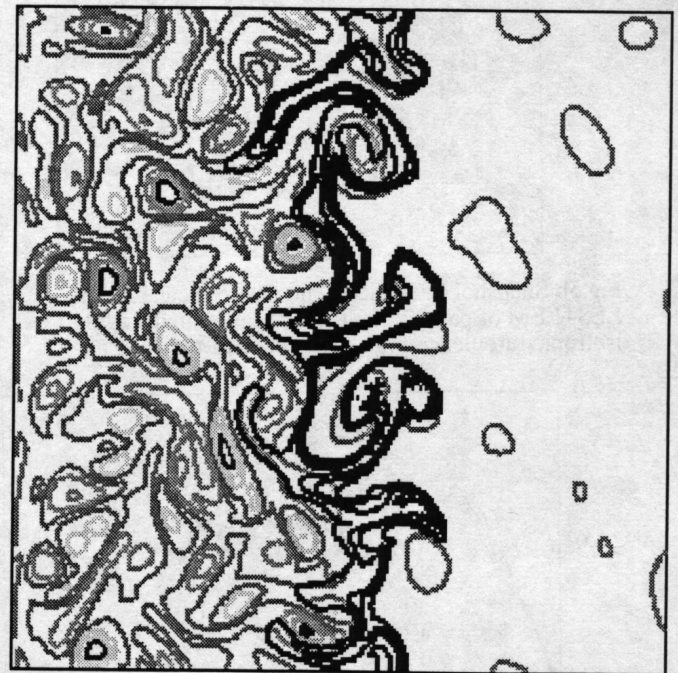
(a)



(b)



(c)



(d)

Fig. 4 DNS of freely propagating premixed flames in homogeneous turbulence. The evolution of species mass fraction from a global finite-rate combustion model is compared with the  $G$ -field equation. Snapshots of vorticity and a) mass fraction at  $\tau=1$ , b) mass fraction at  $\tau=2$ , c)  $G$ -field at  $\tau=1$ , and d)  $G$ -field at  $\tau=2$ .